Published in final edited form as:
*Bone*. 2013 May ; 54(1): 35–43. doi:10.1016/j.bone.2013.01.033.

# Inactivation of Lrp5 in Osteocytes Reduces Young's Modulus and Responsiveness to the Mechanical Loading

**Liming Zhao**[1], **Joon W. Shim**[1], **Todd R. Dodge**[1], **Alexander G. Robling**[1,2], and **Hiroki Yokota**[1,2]

Liming Zhao: lizhao@iupui.edu; Joon W. Shim: shimjoon@iupui.edu; Todd R. Dodge: trdodge@iupui.edu; Alexander G. Robling: arobling@iupui.edu; Hiroki Yokota: hyokota@iupui.edu

[1]Department of Biomedical Engineering, Indiana University Purdue University Indianapolis, IN 46202, USA

[2]Department of Anatomy and Cell Biology, Indiana University School of Medicine, Indianapolis, IN 46202, USA

## Abstract

Low-density-lipoprotein receptor-related protein 5 (Lrp5) is a co-receptor in Wnt signaling, which plays a critical role in development and maintenance of bone. Osteoporosis-pseudoglioma syndrome, for instance, arises from loss-of- function mutations in Lrp5, and global deletion of Lrp5 in mice results in significantly lower bone mineral density. Since osteocytes are proposed to act as a mechanosensor in bone, we addressed a question whether a conditional loss-of-function mutation of Lrp5 selective to osteocytes (Dmp1-Cre; $Lrp5^{f/f}$) would alter responses to ulna loading. Loading was applied to the right ulna for 3 min (360 cycles at 2 Hz) at a peak force of 2.65 N for 3 consecutive days, and the contralateral ulna was used as a non-loaded control. Young's modulus was determined using a midshaft section of the femur. The results showed that compared to age-matched littermate controls, mice lacking Lrp5 in osteocytes exhibited smaller skeletal size with reduced bone mineral density and content. Compared to controls, Lrp5 deletion in osteocytes also led to a 4.6-fold reduction in Young's modulus. In response to ulna loading, mineralizing surface, mineral apposition rate, and bone formation rate were diminished in mice lacking Lrp5 in osteocytes by 52%, 85%, and 69%, respectively. Collectively, the results support the notion that the loss-of-function mutation of Lrp5 in osteocytes causes suppression of mechanoresponsiveness and reduces bone mass and Young's modulus. In summary, Lrp5-mediated Wnt signaling significantly contributes to maintenance of mechanical properties and bone mass.

### Keywords

Lrp5; osteocytes; mechanotransduction; Young's modulus; osteoporosis



Corresponding Author: Hiroki Yokota, PhD, Department of Biomedical Engineering, Indiana University - Purdue University Indianapolis, SL220C, 723 West Michigan Street, Indianapolis, IN 46202, Phone: (317) 278-5177; Fax: (317) 278-2455; hyokota@iupui.edu.

## Introduction

Genetic factors are critical determinants of health and the risk of bone diseases. Extensive genetic and functional data have suggested that a class of secreted morphogenic ligands [1], Wnt proteins, is linked to cellular proliferation and differentiation in numerous tissues [2][3] [4], including bone [5][6]. Wnt signaling is regulated by binding of Wnt ligands to a receptor complex including a low-density-lipoprotein receptor-related protein 5 (Lrp5) [7]. Lrp5 is one of co-receptors for Wnt ligands [8] and genetic mutation involving excess or deficiency in Lrp5 signaling is known to affect bone mass and to increase the risk of bone disorder. A gain-of-function of Lrp5 increases bone mass accrual and strength [9], while null mutations in the receptor reduce bone mineral density [10]. Lrp5 is expressed in many tissues with the highest expression level in the liver [11]. Thus a specific role for Lrp5 in bone tissue is difficult to pinpoint solely based on clinical data or animal models in which its expression is augmented in all tissues [12]. The main aim of this study was to determine the skeletal consequences of Lrp5 deletion selectively in osteocytes and mature osteoblasts.

Skeletal adaptations to weight-bearing activity significantly affect bone's mechanical properties and mass. The removal of regular activity, such as bed rest and microgravity, results in bone loss, commonly referred to as disuse osteoporosis [13]. Postmenopausal osteoporosis and bone fractures are major problems in elderly women, and physical exercise is often recommended to prevent skeletal fragility in age-related osteoporosis [14]. As mechanical signals are able to act as anabolic agents in bone [15] [16], much attention is drawn to an effective use of mechanotransduction or how bone cells transduce physical stimuli to promote new bone formation as a non-drug based intervention for osteoporosis. Although the skeletal consequences of global loss-of-function mutations in Lrp5 are linked to low bone mass [12] [17] [18], the effect of osteocyte-specific deletion of Lrp5 on mechano-responsiveness remains undetermined. In the present study, we investigated the role of Lrp5 in load-driven bone formation by establishing a conditional loss-of-function of Lrp5 selectively in osteocytes.

Two specific questions are addressed in this study: Does osteocytic deletion of Lrp5 alter skeletal size, bone mineral density (BMD), bone mineral content (BMC), and bone material properties (e.g., Young's modulus)? Does osteocytic deletion of Lrp5 suppress responsiveness to load-driven bone formation? To address these questions, we constructed conditional Lrp5 knockout (KO) mutants by breeding dentin matrix acidic phosphoprotein 1 (Dmp1)-Cre mice to Lrp5 floxed mice. We hypothesized that a loss-of-function of Lrp5 in osteocytes would reduce bone size, BMD, BMC, and Young's modulus in adult skeleton, and decrease load-driven bone formation. To evaluate bone size, three-dimensional microstructure, BMD, and BMC, we conducted X-ray imaging using DXA, CT, and pQCT. Young's modulus was determined using dynamic compressive loading to the femur. To test responsiveness to mechanical loading, we employed an ulna loading modality and conducted bone histomorphometry.

## Materials and Methods

### Animals and genotyping

All procedures performed in this study were in accordance with the Institutional Animal Care and Use Committee (IACUC) guidelines. Mice lacking Lrp5 in osteocytes (Dmp1-Cre;$Lrp5^{f/f}$; conditional Lrp5 KO mice) were created by breeding Dmp1-Cre transgenic mice with Lrp5 floxed mice both of which have been described earlier [17] [19]. Briefly, Dmp1 is a transcription factor, expressed predominantly in osteocytes and some latestage osteoblasts [20]. Dmp1-Cre transgenic mice contained a 10 kb fragment of the Dmp1 promoter, which was linked to the coding sequence of Cre recombinase [19]. Lrp5 floxed

mice were engineered to harbor a pair of loxP sequences flanking exon 2 of the Lrp5 gene. Recombination of the floxed allele results in no detectable mRNA. Genotyping was performed using PCR with DNA isolated from tail samples. The primers for detecting Dmp1-Cre (534 bp product) were: 5'-CCC GCA GAA CCT GAA GAT G-3', and 5'-GAC CCG GCA AAA CAG GTA G-3'. The primers for testing the presence of an Lrp5-floxed region were: 5'-TCT TGT AGC ACC CAG GAC CAT C-3' (forward 1), 5'-TGC TCT TTC ATG CCC TCA GTG TA-3' (forward 2), and 5'-CAC CAC AGC CAA CAG TCA CAG A-3' (reverse for both forwards 1 and 2). Note that the forward primer 1 generated 404-bp PCR products ($Lrp5^{f/f}$) and 282-bp PCR products (wild type control), while the forward primer 2 produced 534-bp cDNA fragments (Dmp1-Cre;$Lrp5^{f/f}$) and 3,435 bp cDNA fragments including exon 2 of Lrp5 (wild type).

### RNA isolation and real-time PCR

Total RNA was isolated from the femora of 4 week-old mice. In brief, the femora were stripped of surrounding tissues and periosteum. Their distal and proximal ends were cut off, and medullary cavities were rinsed with a saline solution. The femur samples were homogenized by a tissue homogenizer, and total RNA was isolated using TRIzol reagent (Life Technologies, Grand Island, NY, USA) and purified using Qiagen RNeasy mini kit. Using ~ 2 μg of total RNA, reverse transcription was conducted with a high-capacity cDNA reverse transcription kit (Life Technologies, Grand Island, NY, USA). For evaluation of the Lrp5 mRNA levels corresponding to the boundary of exons 1 and 2, quantitative real-time PCR was performed using a TaqMan gene expression master mix kit. The Lrp5 mRNA level at the boundary of exons 1 and 2 was normalized using the level of GAPDH mRNA.

### Western Blot Analysis

Femur samples were dissociated with a mortar and pestle in a RIPA lysis buffer containing protease inhibitors (Calbiochem). Isolated proteins were fractionated using 10% SDS gels, and wet- and semidry-transferred to Immobilon-P membranes (Millipore) for Lrp5 and β actin, respectively. Membranes were incubated with primary antibodies specific to Lrp5 (Cell Signaling) or β-actin (Sigma), followed by secondary antibodies conjugated with HRP. Signals were detected with ECL chemiluminescence, and images were captured using an image analyzer (LAS-3000, Fuji Photo Film).

### Longitudinal radiography

Radiographs of 16-week-old mice were obtained using a highresolution digital X-ray machine (piXarray100, Tucson, AZ, USA). Mice were anesthetized via inhalation of 2.5% isoflurane (IsoFlo; Abbott Lab, North Chicago, IL, USA) mixed with $O_2$ (1.5 L/min), and they were placed in a prone position (facing to an X-ray sensor). The lateral and posterior images were acquired at 45 kV and 1 sec exposure time, and lengths of the femur and spine (L1 to S5) were measured manually from the digital radiographs using piXarray software.

### Micro computed tomography (μCT)

The femoral mid-diaphysis bone was analyzed using images taken with a high-resolution μCT imaging system (μCT-20; Scanco Medical AG, Basserdorf, Switzerland). From the mid-diaphysis (i.e., 50 % of the total femur length from the tip of femoral condyle to the femur head), 20 transverse slices (6 mm thickness in total) were taken at 60 kV.

### Determination of BMD and BMC

Using peripheral dual-energy X-ray absorptiometry (pDXA; PIXImus II; GE-Lunar Co., Madison, WI, USA), BMD and BMC of a whole body (excluding a head), a section of spine ($L_1$ to $L_5$), and a femur were determined. During scanning, mice (16-week-old) were

anesthetized with isoflurane. Using XCT Research SA+ pQCT (Stratec Electronics, Pforzheim, Germany), volumetric BMD (vBMD) and volumetric BMC (vBMC) of femora were also determined. In brief, bone samples were stored in plastic tubes filled with 70% ethanol, and were positioned in the center of the CT gantry. Using a collimation of 0.26 mm and a voxel size of 0.07 mm, a single slice through each midshaft was imaged. Bone areas and densities were obtained at a threshold of 600 mg/cm$^3$.

### Ulna loading

Mechanical loading was carried out using the ulna loading modality, which has been described previously [12] [21]. In brief, under isoflurane-induced anesthesia, the right ulna was loaded for 3 min (360 cycles at 2 Hz) at a peak force of 2.65 N for 3 consecutive days using an electro actuator (Bose ElectroForce 3200; EnduraTEC, Minnetonka, MN, USA). The left ulna was not loaded and served as an internal control. Intraperitoneal injections of calcein (30 mg/kg body weight; Sigma, Saint Louis, MO, USA) and alizarin (50 mg/kg body weight; Sigma) were administered 5 and 11 days after the first loading day, respectively. Animals were sacrificed 18 days after the first loading day for bone histomorphometry. For strain measurement of the ulna, the previously described method [12] was used. Briefly, the strain gauge was mounted on the lateral face of the ulna, approximately 100 μm from the neutral bending axis of the bone.

### Determination of BMD ratio

Micro CT images of the midshaft of femurs isolated from the control and KO mice were produced using a Skyscan 1172 high-resolution μCT (SkyScan, Kontich, Belgium) at 6-μm resolution. Average density of a 0.05 mm$^3$ rectangular box of cortical bone in each femur was determined using MIMICS 13.1 software (Materialise, Inc., Plymouth, MI, USA). A BMD ratio was created by comparing the average BMD of the KO samples to the average BMD of the controls.

### Determination of Young's modulus

Sections of approximately 5 mm in length were prepared from the femoral midshaft, and dynamic compressive loading was imposed using an ElectroForce 3100 actuator. The loading condition consisted of a ramp function applied at 0.5 N/s to a peak compressive force of 6 N. The maximum load of 6 N was chosen to impart a physiologically relevant strain (~1500 – 2000 μstrain) to the control samples. A loading rate of 0.5 N/s was utilized in order to perform a non-destructive test. Young's modulus was determined using the resulting force-displacement relationship and the physical dimensions of each sample [22].

### Bone histomorphometry

Bone specimens from ulnae were immersed in 10% neutral buffered formalin for 48 h, dehydrated in graded alcohols, cleared in xylene, and embedded in methyl methacrylate. Using a diamond-embedded wire saw (Histo-saw; Delaware Diamond Knives, Wilmington, DE, USA), transverse sections (40 μm) were cut from the midshaft and ground to a final thickness of 20 μm. The slice sections were mounted on slides, and two sections per limb were analyzed using a Bioquant digitizing system (R&M Biometrics, Nashville, TN, USA). The following primary data were collected: total perimeter (B.Pm); single label perimeter (sL.Pm); double label perimeter (dL.Pm); and double label area (dL.Ar). From primary data, we derived mineralizing surface (MS/BS = [1/2sL.Pm+dL.Pm]/B.Pm ×100; %); mineral apposition rate (MAR = dL.Ar/dL.Pm/6 days; μm/day) and bone formation rate (BFR/BS = MAR × MS/BS × 3.65; μm$^3$/μm$^2$ per year). A set of relative values such as rMS/BS, rMAR, and rBFR/BS was derived from the differences between the loaded and nonloaded samples.

### Statistical analysis

Data were expressed as mean ± s.e.m. (standard error of the mean). Differences between the loaded and non-loaded limbs were evaluated using paired t-test. Differences between groups were examined using Student's t test for statistical significance at $p < 0.05$.

## Results

### Construction and characterization of Lrp5 mutant mice

Mice lacking Lrp5 in osteocytes (KO mice) had both positive Dmp1-Cre and homozygous flox allele. To examine whether the genetic engineering strategy was successful in recombining exon 2 of Lrp5 in osteocytes, we conducted PCR-based genotyping for wild type, Lrp5 floxed, and Cre-excised alleles. In the presence of the loxP site in $Lrp5^{f/f}$ mice, we detected 404-bp DNA fragments, which was larger than 282-bp fragments in $Lrp5^{+/+}$ wild type mice in the absence of the loxP site (Fig. 1A, 1B and 1C). Mice lacking Lrp5 in osteocytes (Dmp1-Cre;$Lrp5^{f/f}$) by breeding Dmp1-Cre mice with $Lrp5^{f/f}$ mice yielded 534-bp cDNA products, while their littermate controls generated significantly larger fragments (3,435 bp) including the exon 2 region (Fig. 1B). In the resultant KO mice (Fig. 1C), the Lrp5 mRNA expression at the boundary of exons 1 and 2 in the femurs was significantly diminished (96 % reduction) than that of the littermate controls (Fig. 1D). Immunoblots revealed that the Lrp5 protein level was significantly lower in the femur of KO mice than that of the control (Fig. 1E).

### Shortening of bone length and cortical thickness in the KO mice

The KO mice exhibited an osteopenic skeletal phenotype (Fig. 2A–2B). There was significant reduction in femoral length among KO mice (15.33 ± 0.13 mm; mean ± s.e.m.) as compared controls (15.99 ± 0.23 mm) ($p = 0.044$) (Fig. 2C). Shortening of the spine length ($L_1$ to $S_5$) was also observed (37.34 ± 0.67 mm in control, and 35.44 ± 0.51 mm in KO) ($p = 0.03$) (Fig. 2D). Image analysis exhibited that cortical bone was thinner and more porous in the KO mice than that of the littermate controls (Fig. 3A–3F). Furthermore, the femur of the KO mice showed 21 % reduction in the cross-sectional area compared to Cre-negative littermate controls ($p < 0.01$) (Fig. 3G).

### Reduced BMD and BMC in the KO mice

Compared to the littermate controls, the KO mice exhibited significant reduction in total body BMD (0.052 ± 0.001 g/cm$^2$ in control, and 0.045 ± 0.001 g/cm$^2$ in KO; 15 % decrease) ($p = 0.0005$), femur BMD (0.073 ± 0.002 g/cm$^2$ in control, and 0.061 ± 0.001 g/cm$^2$ in KO; 17 % decrease) ($p = 0.002$), and spine BMD (0.061 ± 0.002 g/cm$^2$ in control, and 0.048 ± 0.002 g/cm$^2$ in KO; 21 % decrease) ($p = 0.0001$) (Fig. 4A–C). Similar effects were noted for total body BMC. The femoral vBMD among KO mice (1096 ± 7 mg/cm$^3$) was significantly lower than that of controls (1169 ± 9 mg/cm$^3$) ($p = 0.0006$). Femoral BMC was likewise reduced among KO mice (0.027 ± 0.0008 mg in control, and 0.018 ± 0.0013 mg in KO) ($p = 0.02$) (Fig. 4D).

### Reduction in Young's modulus in the KO mice

Deletion of Lrp5 in the osteocyte population resulted in altered mechanical properties. The BMD of the KO mice was significantly decreased compared to that of controls, as confirmed by the BMD ratio (less than one), comparing the average BMD of the KO samples to the average BMD of the controls ($p < 0.01$) (Fig. 5A). Also, Young's modulus was reduced from 6.55 ± 0.38 GPa (control) to 1.42 ± 0.24 GPa (KO) ($p = 0.004$) (Fig. 5B). In response to the same bout of cyclic loads, the ulna of the KO mice showed significantly higher strain (3,762 ± 69.6 με) than the littermate control mice (703 ± 34.6 με) ($p < 0.05$) (Fig. 5C).

### Suppression of mechanoresponsiveness in the KO mice

In response to *in vivo* ulna loading, the loaded ulnae of the Cre-negative (control) mice showed fluorescent labeling corresponding to bone formation on the periosteal and endocortical surfaces. However, the ulna of the KO mice presented reduction in fluorescent label incorporation (Fig. 6B). Periosteal mineralizing surface was significantly reduced in the KO mice (31.6 ± 3.1% in control, and 15.2 ± 7.1% in KO) ($p = 0.04$), and mineral apposition rate was decreased significantly (0.74 ± 0.15 μm/day in control, and 0.11 ± 0.12 μm/day in KO) ($p = 0.02$). The relative bone formation rate was 266.8 ± 43.8 $\mu m^3/\mu m^2$ per year in control and 82.2 ± 55.2 $\mu m^3/\mu m^2$ per year in KO ($p = 0.03$) (Fig. 6C). The KO mice also showed a significant decrease in geometric properties. The ulna cortical area was decreased by 10 % (0.253 ± 0.007 AU in control, and 0.228 ± 0.008 AU in KO) ($p < 0.05$), and the minimum cross-sectional moment of inertia was reduced by 16 % (0.0032 ± 0.0001 in control, and 0.0027 ± 0.00009 AU in KO) ($p < 0.05$) (Fig. 6D).

In the periosteal surface, the relative bone formation of the KO mutants was diminished by 27% (227 $\mu m^3/\mu m^2$/yr in control, and 166 $\mu m^3/\mu m^2$/yr in KO) (Fig. 7A). The relationship between relative bone formation rate (y) and strain (x) for the control mice was best-fitted with $y = 0.99x – 466$ ($R^2 = 0.49$) on the periosteal surface.

In the endosteal surface, the relative bone formation rate of the KO mutants was decreased by 66% (196 $\mu m^3/\mu m^2$/yr in control, and 66 $\mu m^3/\mu m^2$/yr in KO) (Fig. 7B). The relationship between relative bone formation rate (y) and strain (x) for the control mice was best-fitted with $y = 1.03x – 528$ ($R^2 = 0.55$) on the endosteum.

The KO mice hardly demonstrated strain-dependent anabolic responses on both periosteum and endosteum, and thus the square of the correlation coefficient was estimated to be 0.11 on the periosteal surface and 0.06 on the endosteal surface (Fig. 7).

## Discussion

We demonstrate in this paper that inactivation of Lrp5 in osteocytes impairs bone mass and size, mechanical properties, and responses to mechanical loading. Compared to the Cre-negative $Lrp5^{f/f}$/ littermates, the conditional Lrp5 KO mice (cre-positive $Lrp5^{f/f}$ mice) lacking functional Lrp5 in osteocytes presented lower BMD and BMC in the whole body, femur and spine. They also presented shorter length of the femur and spine. In response to dynamic loads of 2.65 N to the ulna, the conditional Lrp5 KO mice induced 3,500 to 4,000 strain to the midshaft of the ulna while the littermate controls 500 to 800 μstrain. Although induced strain was significantly higher in response to dynamic loading, bone formation rate was substantially lower both on the periosteal and endosteal surfaces in the conditional Lrp5 KO mice than the littermate controls. These results strongly suggest that Lrp5-mediated Wnt signaling is critical in load-driven bone formation, and maintenance of bone mass and size as well as mechanical properties.

In Wnt-mediated mechanotransduction of bone, the interactions of sclerostin, a negative regulator of bone formation [23], to Lrp5 have been considered to be a key regulatory step [24]. In this mechanism, mechanical loading induces bone formation by repressing transcription of sclerostin, which inhibits Wnt signaling. This hypothesis is in agreement with high bone mass phenotypes in human Lrp5 gain-of-function mutants, in which sclerostin binds less strongly to mutated Lrp5 co-receptors than to wild-type receptors [25]. To further examine the Lrp5-linked mechanism of load-driven bone formation, we developed conditional Lrp5 mutations in the osteocyte pool of mice. Osteocytes reside in lacunae in the bone cortex and are terminally differentiated osteoblasts. In response to mechanical loading, they suppress transcription of sclerostin [26] and elevate synthesis of

Dmp1 for bone mineralization [27]. In the described loss-of-function mutation in Lrp5 gene, the exon 2 was deleted by Cre recombinases driven by a Dmp1-promoter. Dmp1 is essential for mineralization of the skeleton and calcium/phosphate metabolism [28]. It is highly expressed in mature osteoblasts and osteocytes, and Dmp1-Cre mice are reported to activate Cre recombinases predominantly in osteocytes and late stage osteoblasts [29], though a small degree of recombination can also be detected in skeletal muscle in these mice [17]. Together with exons 3 and 4, the exon 2 encodes a YWTD-type β-propeller 1 motif. Lrp5 consists of 4 β-propeller motifs together with 4 epidermal growth factor-like repeats in its extracellular domain [30]. Thus, the described mutation apparently disrupted at least in part binding sites for extracellular Wnt ligands.

The estimation of Young's modulus in the femur by dynamic compressive loading was consistent with the measured strain in the ulna. The proximity to the neutral axis is a major reason why the measured strain was below 1,000 *microstrain*. Strain of the midshaft of long bone is determined by multiple factors including Young's modulus, cross-sectional area, cross-sectional moment of inertia, and bone curvature. Compared to the littermate controls, the conditional Lrp5 KO mice presented 4.6-times smaller Young's modulus, together with 10% reduction in cross-sectional area and 16% decrease in cross-sectional moment of inertia. Bone curvature was not significantly different between the conditional KO and control mice. These geometric and mechanical properties are in good agreement with the induction of significantly higher strain in the conditional KO mice than the littermate control.

The conditional Lrp5 KO mice exhibited similarities and differences to global Lrp5 KO mice that lacked functional Lrp5 throughout the skeletal and non-skeletal system [31]. Since Wnt signaling is involved in morphogenesis of various tissues, impacts on bone shape and stiffness are considered more severe in the global KO mice than the conditional KO mice. However, changes in Young's modulus might be primarily governed by osteocytes through mechanotransduction and thus differences between these two KO strains may differ to a lesser extent [12]. Both global and conditional inactivation of Lrp5 show low bone mass and decreased bone strength. The anabolic response to ulna loading was reduced by ~94% (global KO) and ~78% (conditional KO in this study). Cortical area and cross-sectional moment of inertia in the femur was reduced in both KO mice but the global KO mice to a larger extent (30 to 50%) than the conditional KO mice (10 to 20%).

There are a few limitations in the current study including the design of floxed mice, the target of DMP1 driven Cre mice, and the other receptor in Wnt signaling. First, the described conditional KO strategy aimed to disrupt a part of the extracellular domain in Lrp5 with an intact peptide sequence for the other three -propeller motifs [8][32]. It is thus important to evaluate potential effects of Wnt ligands whose binding to Lrp5 might not be affected by this loss-of-function mutation [33]. Second, Dmp1 driven Cre-recombinase might be activated in mature osteoblasts besides osteocytes. Generating transgenic mice with Cre recombinase driven by, for instance, a type I collagen promoter might be useful [34]. Third, the other known co-receptor, Lrp6, may participate to Wnt signaling and load-driven bone formation. It is yet to be investigated the contributions of Lrp5/6 [8][35]. Last, Wnt signaling has been suggested a therapeutic target for bone diseases [36]. Dickkopf 1 (DKK1), for instance, is known to suppress Wnt signaling by forming a complex with Lrp5/6. Further studies addressing interactions of DKK1 and other Wnt-linked molecules are necessary. In summary, conditional Lrp5 KO mice presented significant decreases in cortical area and cross-sectional moment of inertia, Young's modulus, and mechanosensitivity to load-driven bone formation. The results support the notion that enhancing bone formation by increasing Lrp5-induced signaling may be beneficial to the treatment of osteopenia and osteoporosis.

## Acknowledgments

We dedicate this paper to Charles Turner who provided invaluable guidance and advice throughout this study. We appreciate Bart Williams for providing Lrp5 floxed mice. The study was in part supported from National Institute of Arthritis and Musculoskeletal and Skin Diseases Grant AR53237 (AR) and AR52144 (HY).

## Abbreviations

| | |
|---|---|
| **Lrp5** | low-density-lipoprotein receptor-related protein 5 |
| **Dmp1** | dentin matrix acidic phosphoprotein 1 |
| **Cre** | Cre recombinase |
| **BMD** | bone mineral density |
| **BMC** | bone mineral content |

## References

1. Koay MA, Brown MA. Genetic disorders of the LRP5-Wnt signalling pathway affecting the skeleton. Trends Mol Med. 2005 Mar; 11(3):129–137. Review. [PubMed: 15760771]
2. Flaherty MP, Kamerzell TJ, Dawn B. Wnt signaling and cardiac differentiation. Prog Mol Biol Transl Sci. 2012; 111:153–174. [PubMed: 22917230]
3. Rao TP, Kühl M. An updated overview on Wnt signaling pathways: a prelude for more. Circ Res. 2010 Jun 25; 106(12):1798–1806. [PubMed: 20576942]
4. Niehrs C, Acebron SP. Mitotic and mitogenic Wnt signalling. EMBO J. 2012 May 22; 31(12):2705–2713. [PubMed: 22617425]
5. Marie PJ. Signaling pathways affecting skeletal health. Curr Osteoporos Rep. 2012 Sep; 10(3):190–198. [PubMed: 22711369]
6. Monroe DG, McGee-Lawrence ME, Oursler MJ, Westendorf JJ. Update on Wnt signaling in bone cell biology and bone disease. Gene. 2012 Jan 15; 492(1):1–18. Epub 2011 Nov 3. [PubMed: 22079544]
7. Kubota T, Michigami T, Ozono K. Wnt signaling in bone metabolism. J Bone Miner Metab. 2009; 27(3):265–271. Epub 2009 Mar 31. [PubMed: 19333681]
8. He X, Semenov M, Tamai K, Zeng X. LDL receptor-related proteins 5 and 6 in Wnt/beta-catenin signaling: arrows point the way. Development. 2004 Apr; 131(8):1663–1677. Review. [PubMed: 15084453]
9. Little RD, Carulli JP, Del Mastro RG, Dupuis J, Osborne M, Folz C, et al. A mutation in the LDL receptor-related protein 5 gene results in the autosomal dominant high-bone-mass trait. Am J Hum Genet. 2002 Jan; 70(1):11–19. Epub 2001 Dec 3. [PubMed: 11741193]
10. Gong Y, Slee RB, Fukai N, Rawadi G, Roman-Roman S, Reginato AM, et al. LDL receptor-related protein 5 (LRP5) affects bone accrual and eye development. Cell. 2001 Nov 16; 107(4): 513–523. [PubMed: 11719191]
11. Hey PJ, Twells RC, Phillips MS, Yusuke Nakagawa, Brown SD, Kawaguchi Y, et al. Cloning of a novel member of the low-density lipoprotein receptor family. Gene. 1998 Aug 17; 216(1):103–111. [PubMed: 9714764]
12. Sawakami K, Robling AG, Ai M, Pitner ND, Liu D, Warden SJ, et al. The Wnt co-receptor LRP5 is essential for skeletal mechanotransduction but not for the anabolic bone response to parathyroid hormone treatment. J Biol Chem. 2006 Aug 18; 281(33):23698–23711. Epub 2006 Jun 20. [PubMed: 16790443]
13. Giangregorio L, Blimkie CJ. Skeletal adaptations to alterations in weight-bearing activity: a comparison of models of disuse osteoporosis. Sports Med. 2002; 32(7):459–476. [PubMed: 12015807]

14. Srinivasan S, Gross TS, Bain SD. Bone mechanotransduction may require augmentation in order to strengthen the senescent skeleton. Ageing Res Rev. 2012 Jul; 11(3):353–360. Epub 2012 Jan 5. [PubMed: 22240208]
15. Ozcivici E, Luu YK, Adler B, Qin YX, Rubin J, Judex S, et al. Mechanical signals as anabolic agents in bone. Nat Rev Rheumatol. 2010 Jan; 6(1):50–59. [PubMed: 20046206]
16. Zhang P, Sun Q, Turner CH, Yokota H. Knee loading accelerates bone healing in mice. J Bone Miner Res. 2007 Dec; 22(12):1979–1987. [PubMed: 17696761]
17. Cui Y, Niziolek PJ, MacDonald BT, Zylstra CR, Alenina N, Robinson DR, et al. Lrp5 functions in bone to regulate bone mass. Nat Med. 2011 Jun; 17(6):684–691. Epub 2011 May 22. [PubMed: 21602802]
18. Korvala J, Jüppner H, Mäkitie O, Sochett E, Schnabel D, Mora S, et al. Mutations in LRP5 cause primary osteoporosis without features of OI by reducing Wnt signaling activity. BMC Med Genet. 2012 Apr 10.13:26. [PubMed: 22487062]
19. Lu Y, Xie Y, Zhang S, Dusevich V, Bonewald LF, Feng JQ. DMP1-targeted Cre expression in odontoblasts and osteocytes. J Dent Res. 2007 Apr; 86(4):320–325. [PubMed: 17384025]
20. Wesseling-Perry K. FGF-23 in bone biology. Pediatr Nephrol. 2010 Apr; 25(4):603–608. Epub 2009 Dec 15. Review. [PubMed: 20012997]
21. Torrance AG, Mosley JR, Suswillo RF, Lanyon LE. Noninvasive loading of the rat ulna in vivo induces a strain-related modeling response uncomplicated by trauma or periostal pressure. Calcif Tissue Int. 1994 Mar; 54(3):241–247. [PubMed: 8055374]
22. Eddleston A, Marenzana M, Moore AR, Stephens P, Muzylak M, Marshall D, et al. A short treatment with an antibody to sclerostin can inhibit bone loss in an ongoing model of colitis. J Bone Miner Res. 2009 Oct; 24(10):1662–1671. [PubMed: 19419292]
23. Papapoulos SE. Targeting sclerostin as potential treatment of osteoporosis. Ann Rheum Dis. 2011 Mar; 70(Suppl 1):i119–i122. Review. [PubMed: 21339215]
24. Ellies DL, Viviano B, McCarthy J, Rey JP, Itasaki N, Saunders S, et al. Bone density ligand, Sclerostin, directly interacts with LRP5 but not LRP5G171V to modulate Wnt activity. J Bone Miner Res. 2006 Nov; 21(11):1738–1749. [PubMed: 17002572]
25. Balemans W, Piters E, Cleiren E, Ai M, Van Wesenbeeck L, Warman ML, Van Hul W. The binding between sclerostin and LRP5 is altered by DKK1 and by high-bone mass LRP5 mutations. Calcif Tissue Int. 2008 Jun; 82(6):445–453. [PubMed: 18521528]
26. van Oers RF, van Rietbergen B, Ito K, Hilbers PA, Huiskes R. A sclerostin-based theory for strain-induced bone formation. Biomech Model Mechanobiol. 2011 Oct; 10(5):663–670. Epub 2010 Nov 11. [PubMed: 21069416]
27. Tu X, Rhee Y, Condon KW, Bivi N, Allen MR, Dwyer D, et al. Sost downregulation and local Wnt signaling are required for the osteogenic response to mechanical loading. Bone. 2012 Jan; 50(1):209–217. Epub 2011 Oct 30. [PubMed: 22075208]
28. Ling Y, Rios HF, Myers ER, Lu Y, Feng JQ, Boskey AL. DMP1 depletion decreases bone mineralization in vivo: an FTIR imaging analysis. J Bone Miner Res. 2005 Dec; 20(12):2169–2177. Epub 2005 Aug 22. [PubMed: 16294270]
29. Harris SE, MacDougall M, Horn D, Woodruff K, Zimmer SN, Rebel VI, et al. Meox2Cre-mediated disruption of CSF-1 leads to osteopetrosis and osteocyte defects. Bone. 2012 Jan; 50(1):42–53. Epub 2011 Sep 20. [PubMed: 21958845]
30. Takagi J, Yang Y, Liu JH, Wang JH, Springer TA. Complex between nidogen and laminin fragments reveals a paradigmatic beta-propeller interface. Nature. 2003 Aug 21; 424(6951):969–974. [PubMed: 12931195]
31. Yadav VK, Ryu JH, Suda N, Tanaka KF, Gingrich JA, Schütz G, Glorieux FH, Chiang CY, Zajac JD, Insogna KL, Mann JJ, Hen R, Ducy P, Karsenty G. Lrp5 controls bone formation by inhibiting serotonin synthesis in the duodenum. Cell. 2008 Nov 28; 135(5):825–837. [PubMed: 19041748]
32. Balemans W, Van Hul W. The genetics of low-density lipoprotein receptor-related protein 5 in bone: a story of extremes. Endocrinology. 2007 Jun; 148(6):2622–2629. Epub 2007 Mar 29. [PubMed: 17395706]
33. Baron R, Rawadi G, Roman-Roman S. Wnt signaling: a key regulator of bone mass. Curr Top Dev Biol. 2006; 76:103–127. Review. [PubMed: 17118265]

34. Ono N, Nakashima K, Schipani E, Hayata T, Ezura Y, Soma K, et al. Constitutively active PTH/PTHrP receptor specifically expressed in osteoblasts enhances bone formation induced by bone marrow ablation. J Cell Physiol. 2012 Feb; 227(2):408–415. [PubMed: 21866553]

35. Zhong Z, Baker JJ, Zylstra-Diegel CR, Williams BO. Lrp5 and Lrp6 play compensatory roles in mouse intestinal development. J Cell Biochem. 2012 Jan; 113(1):31–38. [PubMed: 21866564]

36. Hoeppner LH, Secreto FJ, Westendorf JJ. Wnt signaling as a therapeutic target for bone diseases. Expert Opin Ther Targets. 2009 Apr; 13(4):485–496. [PubMed: 19335070]

## Highlights

- Selective inactivation of Lrp5 in osteocytes in mice shows reduced bone mass.
- Inactivation of Lrp5 in osteocytes leads to 4.6 times lower Young's modulus in the femur.
- Mice lacking Lrp5 in osteocytes present significantly diminished load-driven bone formation.

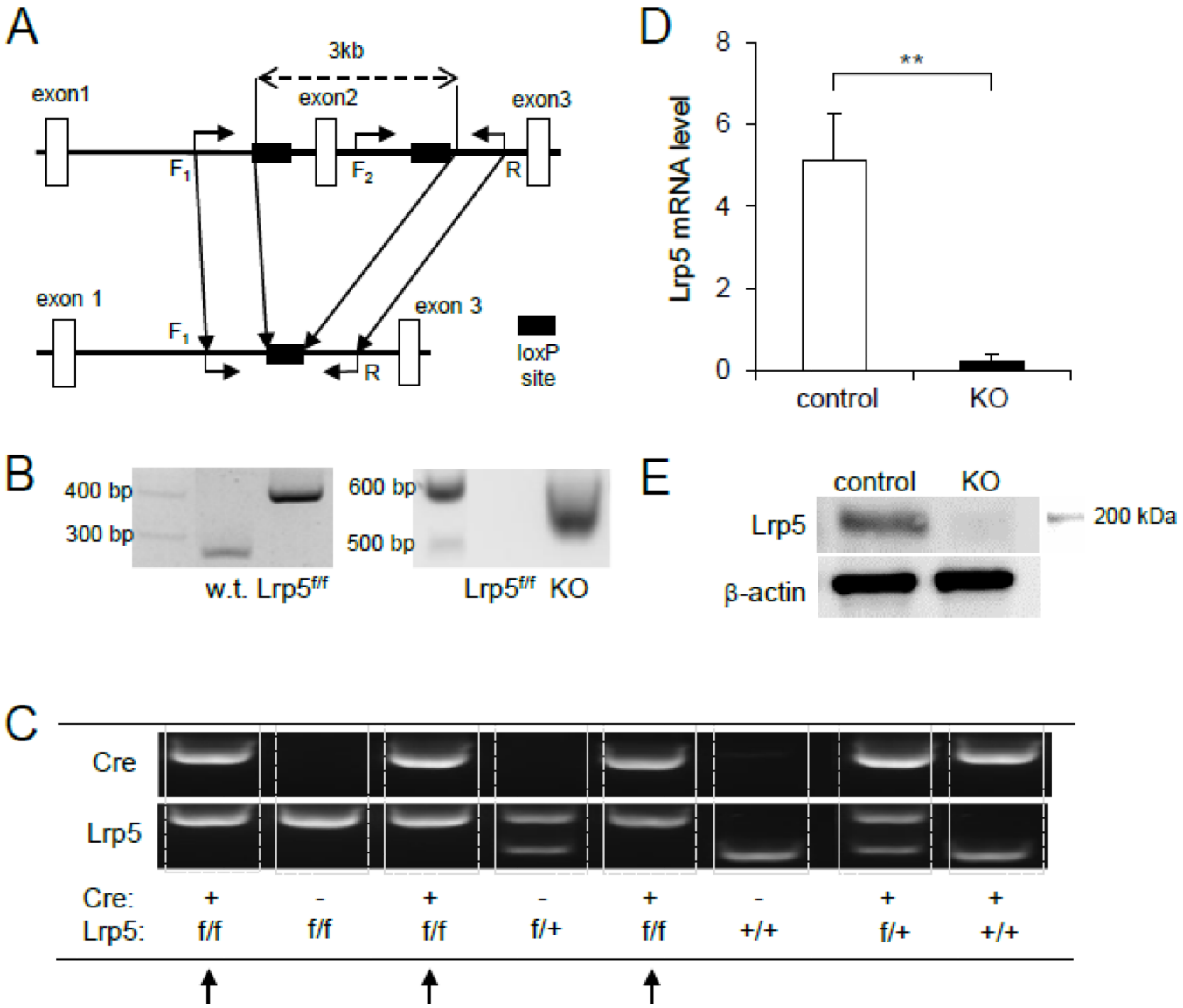


**Fig. 1.**

Characterization of mice with a conditional Lrp5 knockout allele by breeding mice homozygous for Lrp5 floxed ($Lrp5^{f/f}$) with Dmp1-Cre mutants (Dmp1-Cre;$Lrp5^{f/f}$). (A) Schematic depicting the construction of the Lrp5 floxed allele on the basis of exon 2 region, flanked by a pair of loxP sites. Shown here are loxP sites (solid rectangle), the size of regions of interest involving exon 2 prior to recombination (3 kb, dashed arrow) and exon 1,2 and 3 (open rectangle). The relative locations and orientation of the primers (forward as in $F_1$-$F_2$, and reverse as in R; solid arrows) used for PCR genotyping are denoted. The expected size of base-pair (bp) is 282 bp (w.t.), 404 bp (floxed), and 534 bp (Dmp1-Cre). (B) Different genotypes on agarose gel displaying amplified PCR products for w.t., floxed (f/f) and Lrp5 knockout (−/−) alleles after flippase and Cre excision using genomic DNA of mice. Abbreviated w.t. denotes wild-type mice. (C) Photograph of genotyping for mice in the absence or presence of Lrp5 floxed allele with or without the Dmp1-Cre transgene. Lrp5 conditional knockout (KO) is marked with arrows ($Lrp5^{f/f}$ with Dmp1-$Cre^{+}$). Mice genotyped as $Lrp5^{f/f}$ with Dmp1-$Cre^{-}$ was used as control in comparison with KO or $Lrp5^{-/-}$ ($Lrp5^{f/f}$ with Dmp1-$Cre^{+}$). (D) Graph depicting relative abundance of Lrp5 mRNA

expression in bone (ulna) of 16-week-old mice homozygous (f/f) for floxed Lrp5 alleles with (Dmp1-Cre$^{+}$) and without Dmp1-Cre transgene (Dmp1-Cre$^{-}$). Relative quantification was conducted by normalization to the internal reference, glyceraldehyde 3- phosphate dehydrogenase (GAPDH). n=9 for control and n=5 for KO mice. The error bars denote means ± s.e.m. The double asterisks, **, indicate $p<0.01$ with respect to floxed Lrp5 littermates that were negative for the Cre transgene (Dmp1-Cre$^{-}$). (E) Lrp5 protein levels in the right femurs of the control and KO mice.

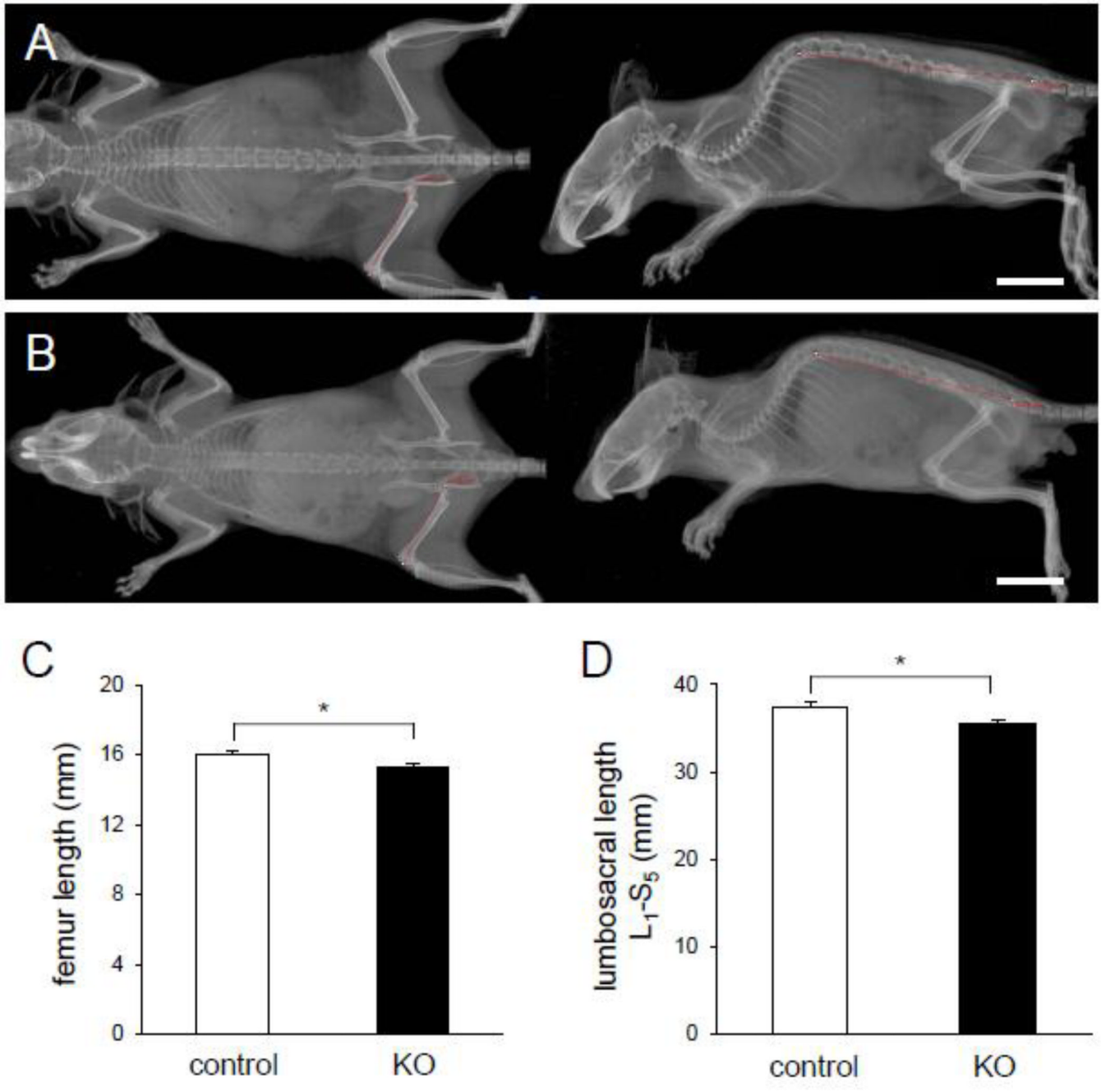


**Fig. 2.**

Sizes of the skeletal system for mice lacking Lrp5 in osteocytes and littermate control (16 week old) including an appendicular and axial skeleton. (A) Radiograph of a littermate control ($Lrp5^{f/f}$ with Dmp1-$Cre^{-}$). (B) Radiograph of a mouse lacking Lrp5 in osteocytes ($Lrp5^{f/f}$ with Dmp1-$Cre^{+}$). The trace of femur as an appendicular skeleton and lumbosacral ($L_1$ to $S_5$ or spine to pelvis bone) as an axial skeleton is indicated in the red curve. White scale bars, 10 mm in (AB). (C) Graph depicting comparison of the appendicular skeleton by measuring length of the long bone (femoral) in the littermate control and KO mice. (D) Graph depicting comparison of the axial skeleton by measuring length of the lumbosacral

spine line, $L_1$ to $S_5$, in the littermate control and KO mice. n=9 for control and n=5 for KO mice. The error bars denote means ± s.e.m. The asterisk,*, indicates $p < 0.05$.

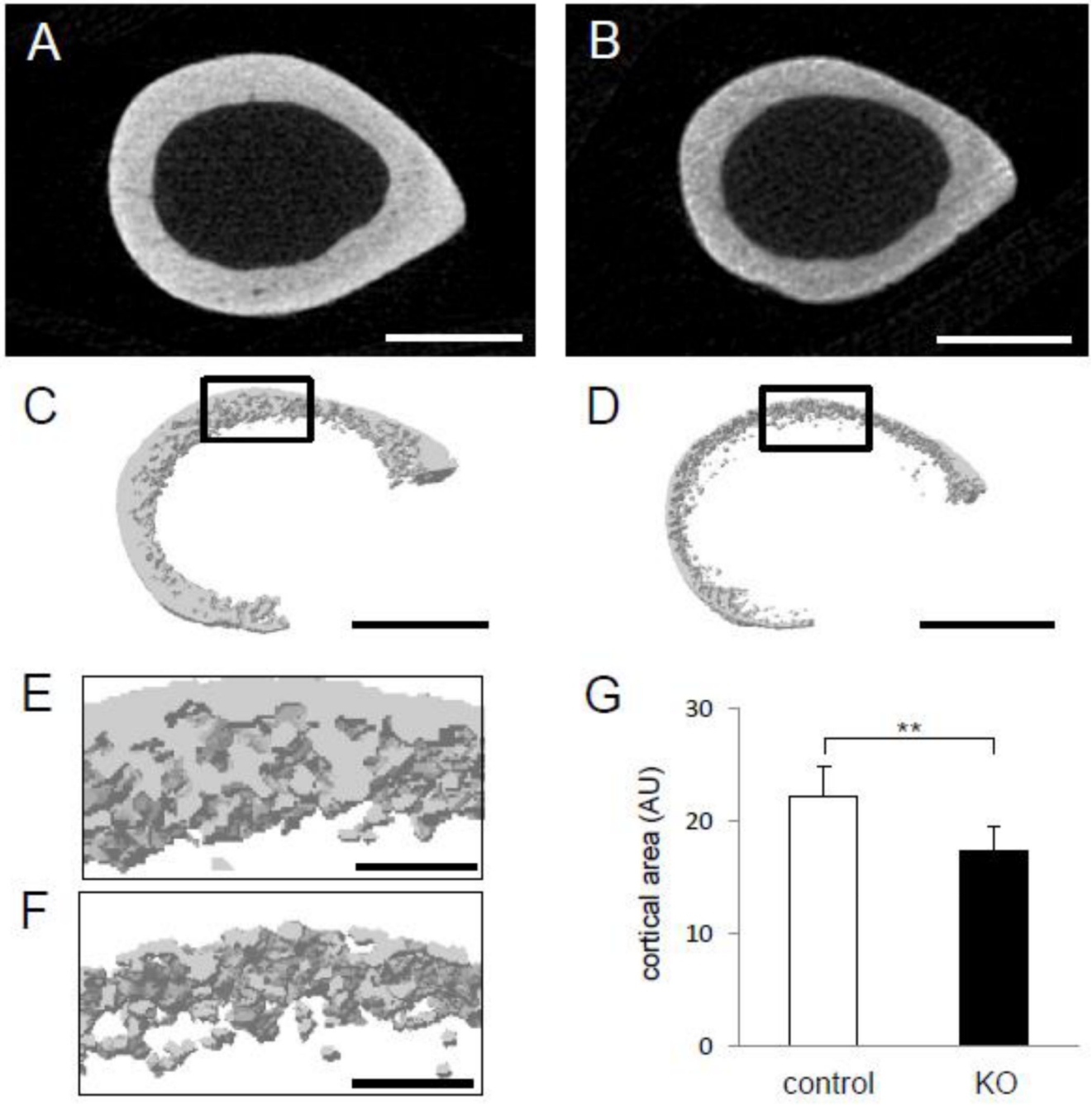


**Fig. 3.**

Photographs of μCT images on an appendicular skeleton. (A) Cross section of the femoral middle shaft in littermate controls ($Lrp5^{f/f}$). (B) Cross section of the femoral middle shaft in mice lacking Lrp5 in osteocytes ($Lrp5^{-/-}$). (C) 3D-reconstructed image of the midshaft section of littermate controls ($Lrp5^{f/f}$). (D) 3D-reconstructed image of the midshaft section of mice lacking Lrp5 in osteocytes ($Lrp5^{-/-}$). Scale bar = 500 μm in (A–D). (E) Magnified view of the focused (black rectangle) area in control animals depicting quality of cortical bone. (F) Magnified view of the focused (black rectangle) area in mice lacking Lrp5 in osteocytes depicting disrupted quality of cortical bone. (G) Graph depicting the cortical area of cross section of the femur by subtracting area of medullar cavity from the whole cross

section. AU denotes arbitrary units or pixel$^2$. n=9 for control and n=5 for KO mice. The error bars denote means ± s.e.m. The double asterisks, **, indicate $p < 0.01$. Scale bar = 100 μm in (E–F).

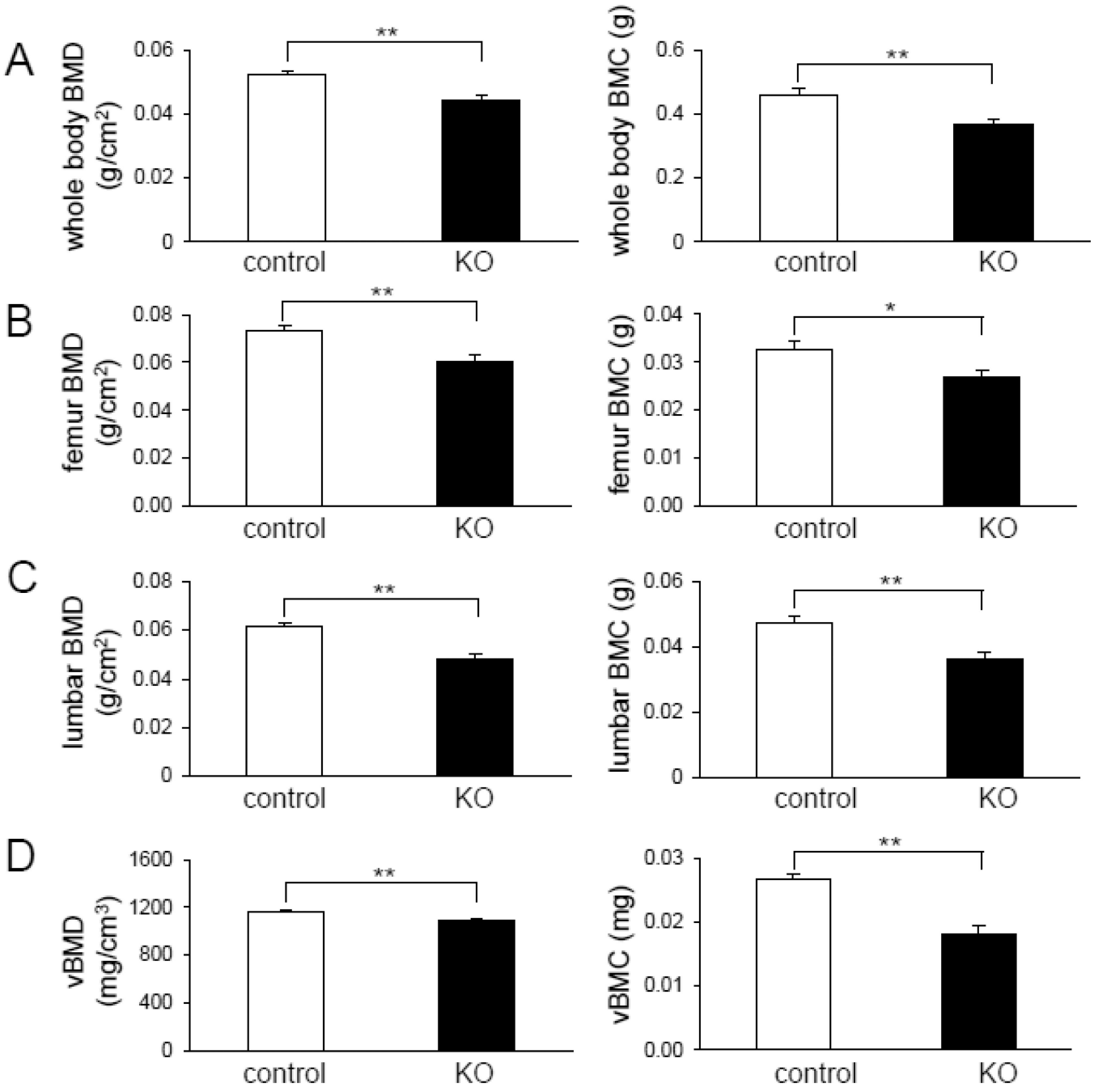


**Fig. 4.**

Effect of Lrp5 deficiency in osteocytes on bone mass. (A) Graphs depicting whole-body BMD (left) and BMC (right) in 16-week-old mice homozygous for floxed Lrp5 allelles, in the absence or presence of the Dmp1-Cre transgene ($Lrp5^{f/f}$ and $Lrp5^{-/-}$, respectively). (B) Graphs depicting right femoral BMD (left) and BMC (right) in 16-week-old mice homozygous for floxed Lrp5 allelles, in the absence or presence of the Dmp1-Cre transgene ($Lrp5^{f/f}$ and $Lrp5^{-/-}$, respectively). (C) Graphs depicting lumbar BMD (left) and BMC (right) in 16-week-old mice homozygous for floxed Lrp5 allelles, in the absence or presence of the Dmp1-Cre transgene ($Lrp5^{f/f}$ and $Lrp5^{-/-}$, respectively). (D) Graphs depicting volumetric BMD (left) and BMC (right) of the femoral middle shaft in 16-week-old mice

homozygous for floxed Lrp5 allelles, in the absence or presence of the Dmp1-Cre transgene ($Lrp5^{f/f}$ and $Lrp5^{-/-}$, respectively). n=9 for control and n=5 for KO mice. The error bars show means ± s.e.m. The single, *, and double asterisks, **, indicate $p < 0.05$ and $p < 0.01$, respectively.

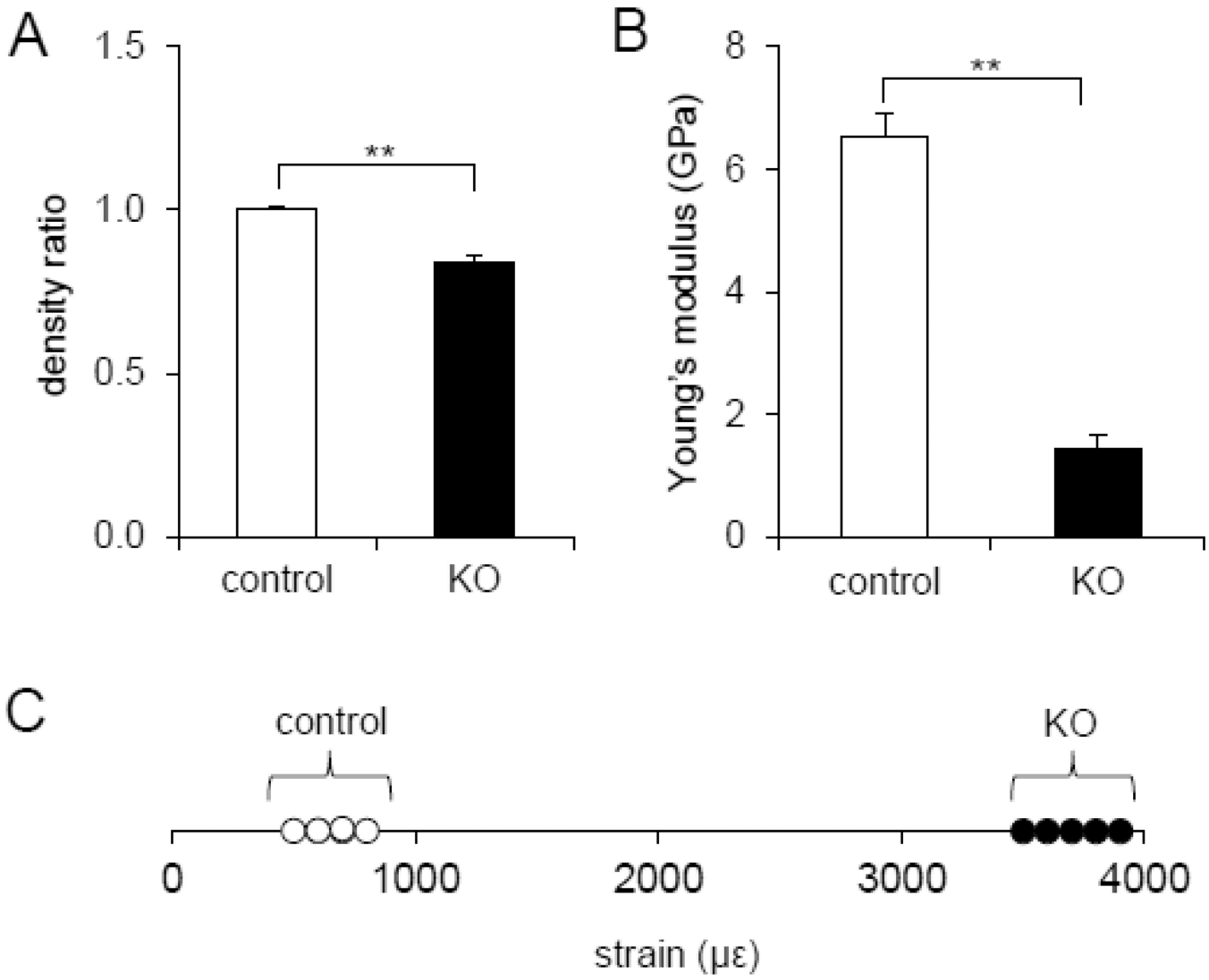


**Fig. 5.**

Quantification of bone density, Young's modulus, and ability to deform in response to mechanical loading. (A) Graph depicting bone density ratio to control values in the midshaft femur of littermate control and mice lacking Lrp5 in osteocytes. (B) Graph depicting Young's modulus obtained from force-displacement curve of a compressive loading experiment using midshaft of the femur in the control and mice lacking Lrp5 in osteocytes. The double asterisks denote $p<0.01$ (A–B). n=8 for control and n=5 for KO mice in (A–B). (C) Graph depicting strain values measured from ulnae of each mouse group in response to the applied compressive loading at 2.65 N in littermate controls and mice lacking Lrp5 in osteocytes. Note that the range of strains in littermate controls fall near 1000 με, while the mice lacking Lrp5 in osteocytes near 4000 με. n=4 for control and n=5 for KO mice.

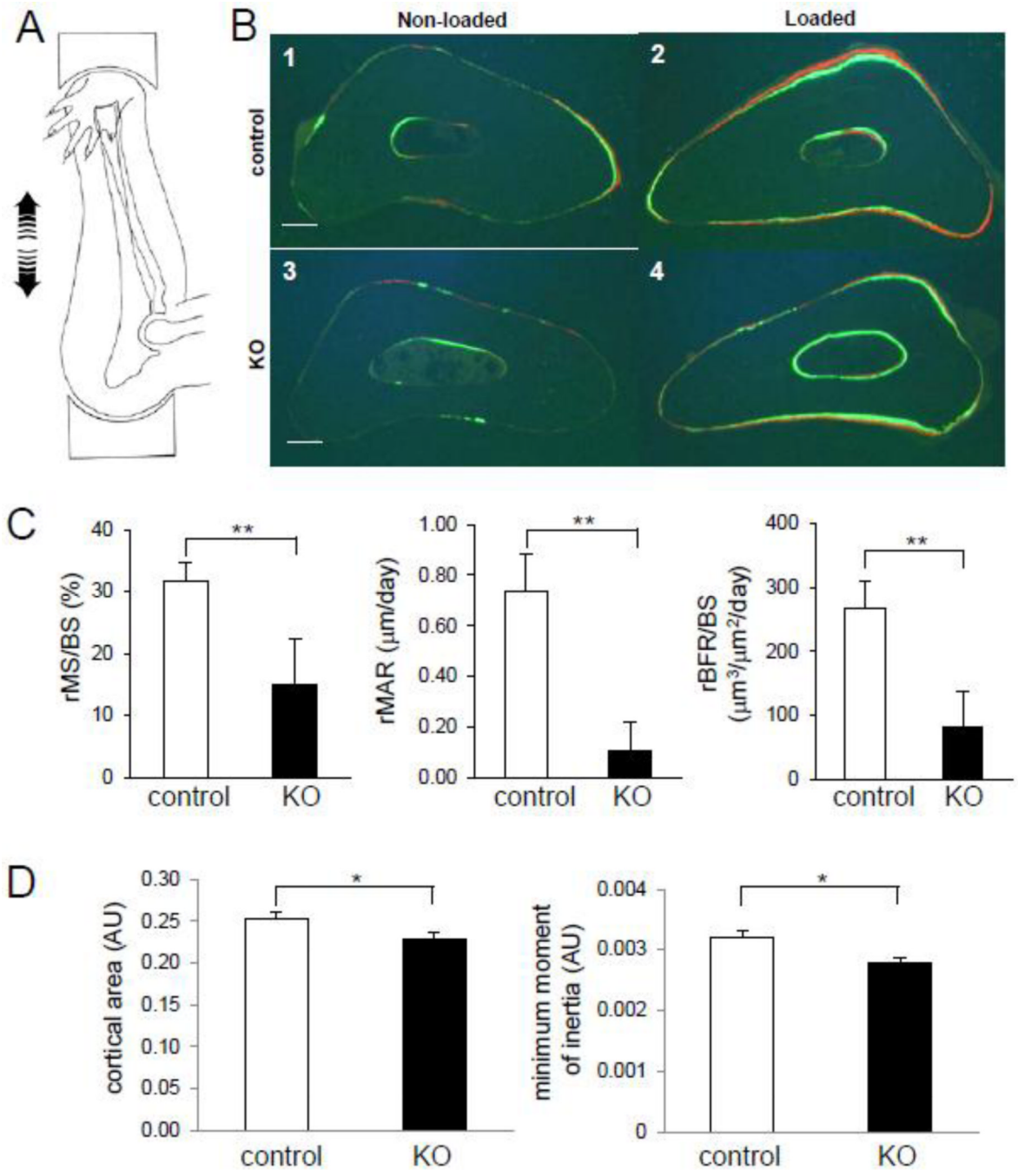


**Fig. 6.**

Response to ulna loading in mice lacking Lrp5 in osteocytes. (A) Diagram illustrating the mouse ulna loading modality. Cyclic compression is applied to the forearm, which generates bending. (B) Cross sections of middle-shaft ulna in the absence or presence of loading among littermate controls and mice lacking Lrp5 in osteocytes. The green and red fluorescent signals are labeled with calcein and alizarin, respectively. B1: nonloaded ulna (littermate controls), B2: loaded ulna (littermate controls); B3: nonloaded ulna (mice lacking Lrp5 in osteocytes); and B4: loaded ulna (mice lacking Lrp5 in osteocytes). Scale bar = 0.1 mm in (B1–B4). (C) Graphs depicting relative mineralizing surface per bone surface (rMS/BS), relative mineral apposition rate (rMAR), and relative bone formation rate per bone

surface (rBFR/BS) in the ulna of 16- week old littermate controls and mice lacking Lrp5 in osteocytes. (D) Graphs depicting cortical area of the cross section in ulna, and the minimum cross-sectional moment of inertia around the major axis out of the ellipsoidal donut-like cross section of the ulna in 16–week–old littermate controls and mice lacking Lrp5 in osteocytes. AU denotes arbitrary units of $pixel^2$ for cortical area and $pixel^4$ for the minimum cross-sectional moment of inertia, respectively. n=8 for control and n=5 for KO mice in (C–D). The error bars show means ± s.e.m. * $p < 0.05$, ** $p < 0.01$ (CD).

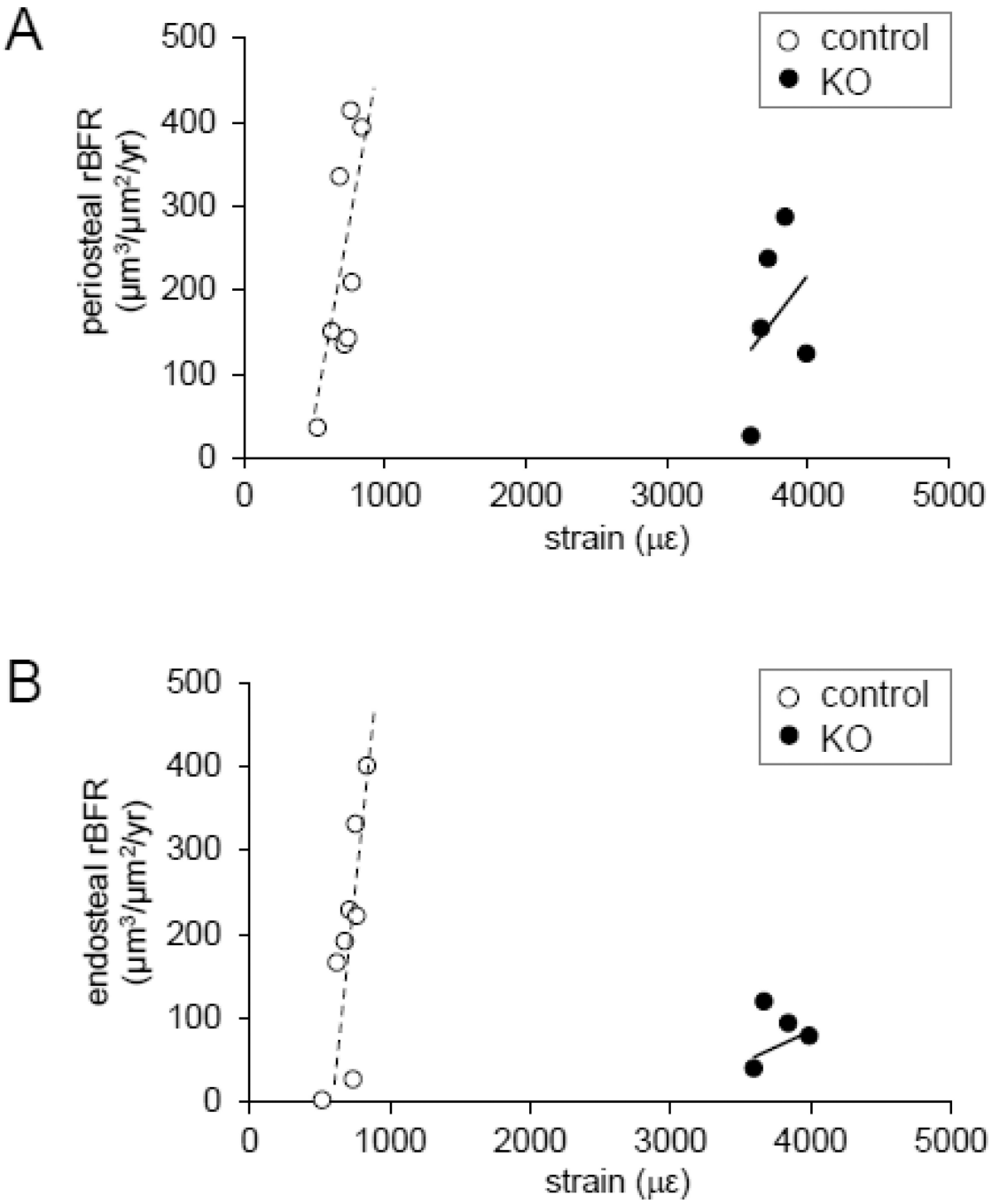


**Fig. 7.**

Ability to respond to normal tissue strains for mice lacking Lrp5 in osteocytes. (A) Graph depicting relative bone formation rate (rBFR) on the periosteal surface of the middle shaft ulna in response to applied mechanical strain in mice lacking Lrp5 in osteocytes as compared to the littermate controls. The dotted and solid lines denote linear regression and the coefficient of determination for controls and KO mice, respectively ($y = 0.99x – 466$, $R^2 = 0.49$). (B) Graph depicting relative bone formation rate (rBFR) on the endosteal surface of the middle shaft ulna in response to applied mechanical strain in mice lacking Lrp5 in osteocytes as compared to the littermate controls. The dotted and solid lines denote linear

regression and the coefficient of determination for controls and KO mice, respectively ($y = 1.03x – 528$, $R^2 = 0.55$).